

The qspec Python package: A physics toolbox for laser spectroscopy

P. Müller^{a,1,*}, W. Nörtershäuser^{a,b}

^a*Institut für Kernphysik, Technische Universität Darmstadt, 64289, Darmstadt, Germany*

^b*Helmholtz Research Academy Hesse for FAIR, Campus Darmstadt, 64289, Darmstadt, Germany*

Abstract

The analysis of experimental results with Python often requires writing many code scripts which all need access to the same set of functions. In a common field of research, this set will be nearly the same for many users. The qspec Python package was developed to provide functions for physical formulas, simulations and data analysis routines widely used in laser spectroscopy and related fields. Most functions are compatible with numpy arrays, enabling fast calculations with large samples of data. A multidimensional linear regression algorithm enables a King plot analyses over multiple atomic transitions. A modular framework for constructing lineshape models can be used to fit large sets of spectroscopy data. A simulation module within the package provides user-friendly methods to simulate the coherent time-evolution of atoms in electro-magnetic fields without the need to explicitly derive a Hamiltonian.

Keywords: Laser spectroscopy, Python, Data analysis, Multidimensional linear regression, Maximum likelihood fitting, Master equation

1. Introduction

The method of laser spectroscopy and the interaction of light with atoms in general is used in many research applications. These range from collinear laser spectroscopy (CLS) to probe atomic or nuclear structure theory [1–6], over searches for new physics [7, 8], the development of atomic clocks [9–11], to quantum computing [12–14]. During the planning or the analysis phase, most of these applications require simulations of the time evolution of atoms in laser fields, nonlinear fits to spectroscopy data or simple calculations of energies, velocities, Doppler shifts, hyperfine-structure (hfs) shifts, *etc.*

The qspec package uses well-established theory and methods for its physics calculations and provides them in a user-friendly way. Whenever useful, functions are compatible with the ndarray class of numpy [15]. This enables fast calculations with large samples of data. In addition to numpy, a small number of established scientific Python packages are required with scipy [16], sympy [17] and matplotlib [18]. The content of the qspec package is distributed over seven modules. These are named `analyze`, `algebra`, `models`, `physics`, `simulate`, `stats`, and `tools`. Parts of qspec are written in C++ and are currently only compiled for Windows systems in a Dynamic Link Library (DLL) for 32 and 64-bit systems. A detailed API documentation of qspec can be found on the Python Package Index (PyPI) [19] and supplemental details are given in [20]. The following paragraphs give a short overview over the different modules.

1.1. algebra

The `algebra` module is a collection of functions related to angular momentum coupling such as Wigner- j symbols, reduced dipole matrix elements and relative transition strengths for electronic transitions. This is the only module that uses the sympy package to return algebraic expressions of coupling strengths.

1.2. analyze

The `analyze` module contains general purpose routines for (non)linear data fitting as well as a convenience class for multi-dimensional King plots [21]. Wrappers for the `scipy.optimize.curve_fit` and the `scipy.odr.odr` routine, which use least square optimization and orthogonal distance regression, respectively [16], extend their functionality and standardize their syntax. For fitting of a straight line, as needed in King-plots, the York algorithm described in [22] and the Monte-Carlo (MC) method described in the supplementary material of [23] are implemented. In both cases, also a generalized version is implemented for fitting a straight line to data points in multiple dimensions, which are distributed according to independent multivariate normal distributions. The multidimensional fit algorithms are described in Sec. 2.

1.3. models

The `models` module contains classes and helper functions to create lineshape models of fluorescence spectra or more general fit models for nonlinear curve-fitting. This module is similar to the existing `satlas2` Python package [24, 25], which is widely used by laser spectroscopy groups at KU Leuven, CERN/ISOLDE and JYVL. In `models`, additional features

*Corresponding author

Email address: pmueller@physics.ucla.edu (P. Müller)

¹Present address: Department of Physics and Astronomy, University of California Los Angeles, 90095, Los Angeles, California, USA

such as numerical convolution with commonly used probability density functions, quantum interference (QI) effects [26] or hyperfine-induced mixing [27] are available. The `models` module is described in detail in Sec. 3

1.4. physics

The `physics` module provides physical relations, unit conversions and observables surrounding (collinear) laser spectroscopy such as particle energy and velocity, Doppler, photon recoil, hyperfine structure and Zeeman shifts, refractive indexes, *etc.*

1.5. simulate

The `simulate` module offers an intuitive framework for simulations of laser-atom interactions and is comparable to other packages that simulate the time evolution of quantum systems such as `qutip` [28, 29] or `PyLCP` [30]. Currently, solvers for the Lindblad master, rate and Schrödinger equation as well as a MC solver for the Lindblad master equation are included. The differential photon scattering rate, which also includes quantum interference effects, can be calculated from the density matrix or the state vector. Additionally, a perturbative scattering rate can be calculated, as described in [26]. The `qspect.simulate` module is described in more detail in Sec. 4.

1.6. stats

The `stats` module contains routines for the statistical analysis of data. Besides basic statistical measures such as the (weighted) average or median, the module also provides a MC error propagator. In combination with the nonlinear curve fitters of the `analyze` module, this can be used to calculate uncertainty bands for the fitted function while taking the full covariance matrix into account.

1.7. tools

The `tools` module provides methods for data processing and conversion as well as general mathematical functions. Some examples are the conversion between lists and dictionaries, merging intervals, rounding to n significant decimal places, transforming vectors or printing colored text to the console *etc.*

2. Multidimensional linear regression

The `qspect` package provides an analytical and a MC method for fitting a straight line to data points in k dimensions. For any set of data points $(\vec{X}_i)_{i \in \mathcal{I}}$, with the index set \mathcal{I} , the algorithms described here assume that the real value of the random vector \vec{X}_i is distributed according to an independent multivariate normal distribution $\mathcal{N}(\vec{\mu}_i, \Sigma_i)$, with the mean vector $\vec{\mu}_i \in \mathbb{R}^k$ and the positive-semidefinite covariance matrix $\Sigma_i \in \mathbb{R}^{k \times k}$. Here, we distinguish between an uncertain data point \vec{X}_i , which may be the result of a measurement, and the actual or real but unknown value \vec{x}_i . Figure 1 depicts the optimization problem in 3 dimensions with the resulting straight fit.

The MC approach generates sample vectors \vec{x}_i according to the distributions $\mathcal{N}(\vec{\mu}_i, \Sigma_i)$ under the condition that they are aligned

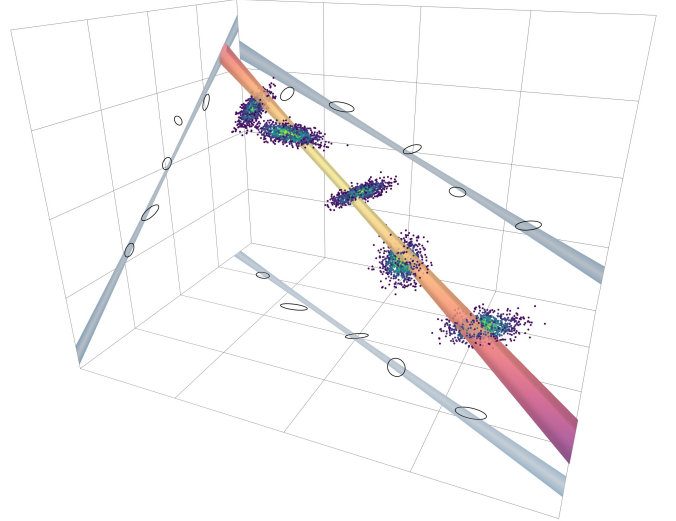


Figure 1: Fit of a straight to 5 data points in 3 dimensions. The scatter plots indicate the uncertainty region of the data points. In the Monte-Carlo (MC) method, similar random samples are generated to construct a distribution of sample straights. The 1σ uncertainty region of the straight fitted with the analytical algorithm is shown as a yellow-purple colormap. The projections of the 1σ uncertainty regions of the data points and the fitted straight are shown on the three orthogonal planes.

on a straight line. Accordingly, the result of the MC method are samples of straights following the probability density function imposed by the uncertain data points and the linear relation. The algorithm is described in detail in the supplemental material of [23] for the 3-dimensional case. However, the extension of this algorithm to k dimensions is straightforward and is, thus, not described here.

The analytical approach is a maximum likelihood fit given the above described assumptions. Its result corresponds to the most probable sample straight generated by the MC method. Note that in general this straight is not given by the mean values of the slopes and y-intercepts of the samples. The algorithm described by York *et al.* [22] yields the analytical solution for 2 dimensions. Here, the extension to k dimensions is not obvious. Hence, in the following, the solution developed for `qspect` is described.

Let a straight in k dimensions be parameterized by

$$f[\vec{a}, \vec{b}] : \mathbb{R} \rightarrow \mathbb{R}^k, \quad t \mapsto \vec{a} + t\vec{b}. \quad (1)$$

Then we want to find the offset vector $\vec{a} \in \mathbb{R}^k$ and the directional vector $\vec{b} \in \mathbb{R}^k$ that define the most likely straight through the set of uncertain data points $(\vec{X}_i)_{i \in \mathcal{I}}$, which generate the independent multivariate normal distributions $\mathcal{N}(\vec{\mu}_i, \Sigma_i)_{i \in \mathcal{I}}$. The probability density of \vec{X}_i can be written as

$$p_i(\vec{x}_i) = \frac{1}{\sqrt{(2\pi)^k |\Sigma_i|}} \exp \left[-\frac{1}{2} (\vec{x}_i - \vec{\mu}_i)^T \Sigma_i^{-1} (\vec{x}_i - \vec{\mu}_i) \right] \quad (2)$$

where T indicates transposition and $|\Sigma_i|$ and Σ_i^{-1} are the determinant and the inverse of the covariance matrix, respectively. We can now define the likelihood of observing a sample \vec{x}_i if it is

constrained to the straight $f[\vec{a}, \vec{b}]$

$$L_i(\vec{a}, \vec{b} | t) := p_i(f[\vec{a}, \vec{b}](t)) \\ = \frac{1}{\sqrt{(2\pi)^k |\Sigma_i|}} \exp \left[-\frac{1}{2} \left(\vec{a}_i^T \Sigma_i^{-1} \vec{a}_i - \frac{t_i^2}{\sigma_i^2} - \frac{(t - t_i)^2}{\sigma_i^2} \right) \right] \quad (3)$$

with the definitions

$$\vec{a}_i := \vec{a} - \vec{\mu}_i, \quad \sigma_i := \frac{1}{\sqrt{\vec{b}^T \Sigma_i^{-1} \vec{b}}}, \quad t_i := -\sigma_i^2 \vec{a}_i^T \Sigma_i^{-1} \vec{b}. \quad (4)$$

The most likely straight can be found by maximizing this likelihood function with respect to \vec{a} and \vec{b} . However, for any given straight $f[\vec{a}, \vec{b}]$, the real value of t that generates \vec{x}_i is unknown. Using

$$\max_{\vec{a}, \vec{b}} L_i(\vec{a}, \vec{b} | t \in \mathbb{R}) = \max_{\vec{a}, \vec{b}} L_i(\vec{a}, \vec{b} | t = t_i) \\ = \max_{\vec{a}, \vec{b}} \frac{1}{\sqrt{(2\pi)^k |\Sigma_i|}} \exp \left[-\frac{1}{2} \left(\vec{a}_i^T \Sigma_i^{-1} \vec{a}_i - \frac{t_i^2}{\sigma_i^2} \right) \right], \quad (5)$$

and recalling that all $(\vec{X}_i)_{i \in I}$ are independent by definition, the likelihood function that needs to be maximized to find the desired straight through all data points is given by

$$L(\vec{a}, \vec{b}) := \prod_{i \in I} L_i(\vec{a}, \vec{b} | t = t_i). \quad (6)$$

Analogously to standard least-square optimization algorithms, this is most efficiently done by minimizing

$$\mathcal{L} := -\log(L(\vec{a}, \vec{b})) \\ = \frac{1}{2} \sum_{i \in I} \log((2\pi)^{k-1} |\Sigma_i|) + \vec{a}_i^T \Sigma_i^{-1} \vec{a}_i - \frac{t_i^2}{\sigma_i^2}, \quad (7)$$

where the terms $\log((2\pi)^{k-1} |\Sigma_i|)$ can be omitted as they are independent of \vec{a} and \vec{b} . In `qspect`, the minimization is performed using the `scipy.optimize.minimize` function with the Newton conjugate gradient (Newton-CG) method [16, 31]. For the fastest possible convergence, in `qspect` both the gradient and the Hessian of Eq. (7) are computed analytically, see [Appendix A](#). The covariance matrix of the resulting \vec{a} and \vec{b} are calculated by numerically inverting the Hessian at the solution with `numpy.linalg.inv`. For 2 dimensions, the algorithm described here reproduces the fit performed with the York algorithm to machine precision. The estimated uncertainties deviate slightly in the third significant digit.

The `qspect` package also contains a class to set up King plots where usually the data vectors, consisting of isotope shifts or nuclear charge radii, are multiplied by mass factors to yield modified data vectors according to

$$\vec{x}_{\text{mod}}^{AA'} = \mu^{AA'} \vec{x}^{AA'} = \frac{(M^A + m_e)(M^{A'} + m_e)}{M^{A'} - M^A} \vec{x}^{AA'}, \quad (8)$$

where M^A is the mass of the nucleus of the isotope with mass number A and m_e is the mass of the electron. The modified

data vectors \vec{x}_{mod} are then aligned on a straight. In this case, the covariance matrices Σ_i are calculated from the masses and data vectors $\vec{x}^{AA'}$. This yields notable positive correlations between the vector components if the uncertainties of the masses are comparable or larger than those of the data vectors. Correlations between different data vectors are neglected. Improved or new data is gained from using the fitted straight to calculate missing vector components j from one known component l

$$x_{\text{mod}}^j = a^j + \frac{b^j}{b^l} (x_{\text{mod}}^l - a^l). \quad (9)$$

The improved unmodified data and their covariance matrix is determined by inverting Eq. (8) and using Gaussian error propagation.

3. Modular fit models

In `qspect.models`, a modular system for constructing fit models, with a focus on lineshape models, is implemented. This module can be compared to the `satlas2` package, which used for fitting lineshape models to low- and high-statistics data [24, 25]. There are several reasons that have lead to the development of `qspect.models`. At the beginning of its development, only the old version of `satlas` was available [24]. Therefore, a large performance boost was expected in `qspect.models`, as evidenced by the now available faster new version `satlas2` [25]. In `qspect.models`, new features and physical models are implemented that were/are not available in `satlas2`, such as consideration of quantum interference effects or convolutions of lineshape models. Moreover, `qspect.models` is now used as the backend of an updated version of the `Tilda.PolliFit` framework, which provides a graphical user interface and is already used for the analyses of online data [32–34]. In the following, the structure of `qspect.models` is described and a performance comparison to `satlas2` is given.

The basis for the modular system is the abstract `Model` class, from which all models inherit. Composite models are created by passing a model to the constructor of another model. A basic example could be the creation of a hyperfine-structure model for a transition from a lower state $|J = 1/2\rangle$ to an upper state $|J' = 3/2\rangle$ in a system with nuclear spin $I = 1/2$

$$f(x) = p_0 \sum_{F \rightarrow F'} a(F, F') \text{Voigt}(x - \bar{x}, \Gamma, \sigma) + y_0 \quad (10) \\ \bar{x} = x_0 + \frac{A'}{2} [F'(F' + 1) - 9/2] - \frac{A}{2} [F(F + 1) - 3/2],$$

where Γ , σ , A , A' , $a(F, F')$, x_0 , p_0 and y_0 are parameters. This would correspond to the following lines of code.

```
1 from qspect.models import \
2     Voigt, Hyperfine, NPeak, Offset
3
4 I, J_l, J_u = 0.5, 0.5, 1.5 # = I, J, J'
5 hfs = Hyperfine(Voigt(), I, J_l, J_u)
6 f = Offset(NPeak(hfs, n_peaks=1))
```

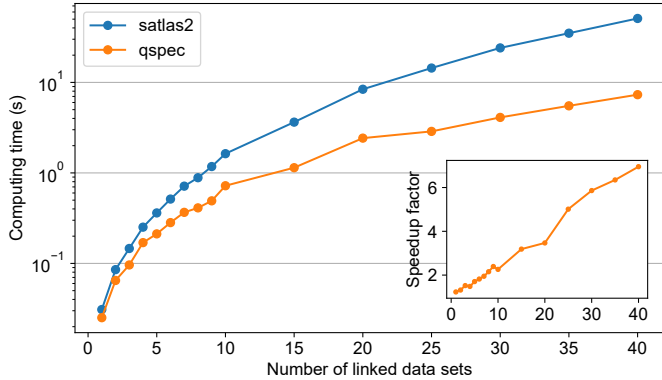


Figure 2: Speed comparison of `qspec.models` with `satlas2` using an adaption of the benchmark test described in the documentation of `satlas2`. The computing time increases polynomially with the number of linked data sets. The ratio of the computing times of `satlas2` and `qspec.models` grows linearly.

Here, Voigt creates the peak shape model with parameters Γ (Lorentzian FWHM) and σ (Gaussian standard deviation) and Hyperfine introduces the sum in Eq. (10), the hyperfine-structure constants A, A' and the peak intensities $a(F, F')$. The NPeak model creates a sum over, in this case, one instance of the passed hyperfine-structure model at the position x_0 with intensity p_0 . The Offset model creates the offset parameter y_0 . The lineshape model defined in Eq. (10) can be substantially modified. The Voigt profile can be replaced by other peak shapes. The chosen peak shape can also be numerically convolved with a second peak shape of choice. The multipole expansion of the hyperfine structure is implemented up to magnetic octupole terms. Quantum interference (QI) effects can be considered by replacing Hyperfine with HyperfineQI. This creates an extra parameter that encapsulates the detector geometry determining the QI effect. Hyperfine-induced mixing is considered in HyperfineMixed. The NPeak model can be used to create additional copies of the passed model with individual position and intensity. The Offset model can be used to divide the x -axis into intervals with individual offset functions. The offset function can be any polynomial. All parameters of a model can be free, fixed, functions of other parameters, bounded to an interval or statistically constraint by a reference value with uncertainty. Additionally, simultaneous fits of multiple data sets with shared parameters are possible. In a future update, `qspec.models` can be combined with the `qspec.simulate` module, described in Sec. 4, to enable fitting of non-perturbative scattering rates. The computing time for a fit with shared parameters increases polynomially with the number of linked data sets. Therefore, the fit models have to be calculated efficiently. To test the speed of `qspec.models`, the benchmark test described in the documentation of `satlas2` [25] was adapted, which compares `satlas2` to `satlas` for fits to different numbers of data sets using shared parameters. There, a speedup factor of two to three orders of magnitude was found, depending on the number of data sets [25]. The benchmark test is a fit of Voigt profiles to the hyperfine structure of a $|J = 1/2\rangle \rightarrow |J' = 3/2\rangle$ transition in a system with nuclear spin $7/2$. The hyperfine-structure parameters A, A' and B' as well as

the parameters x_0, Γ and σ were shared across data sets, compare Eq. (10). The magnetic octupole constant C' was fixed and set to zero. Figure 2 shows a comparison of the computing times of `qspec.models` and `satlas2`. A linearly growing speedup factor of 1.2 to 7 was found for simultaneously fitting 1 to 40 randomly generated data sets, respectively, when using `qspec.models`. The fit results agree well and only deviate in the third significant digit of the uncertainties.

4. Interaction of light and matter

The lineshape of fluorescence spectra cannot always be described by an analytical model, especially when atomic states are optically pumped. In such cases it is desirable to simulate the evolution of the atomic state population in the laser field to understand the origin of the experimental lineshape and to investigate systematic frequency shifts when using a simple lineshape model. Moreover, the simulations can help to find the optimal experimental parameters in experiments that rely on optical pumping effects. All experiments that involve light-atom interactions can potentially benefit from such simulations. Some examples are saturation spectroscopy, Ramsey interferometry or quantum computing with atom/ion traps.

Python packages to simulate the interaction of light and matter already exist. However, they are often designed for a certain subspace of atomic systems and applications or require the user to derive the mathematical objects such as Hamiltonians or observable operators. For example, the `qutip` package is a powerful library of solvers for open quantum systems which takes the Hamiltonian of the system as an input [28, 29]. For the simulation of laser spectroscopy experiments, where multiple isotopes with different hyperfine structures are of interest, a lot of work is required to set up all Hamiltonians. The `PyLCP` package facilitates this process, provides classes to set up lasers and external static electromagnetic fields and also allows to simulate the motional degrees of freedom, *e.g.*, to simulate laser cooling [30]. While this package has a large range of applications, it still requires the user to construct a Hamiltonian from individual energy contributions and it currently does not support passing numpy arrays of velocities or laser detunings to simulate large samples. As a consequence, iterations over the samples and multi-threading for better performance have to be implemented by the user.

The `qspec.simulate` module provides an intuitive class system, which is comparable to drawing an atomic level scheme, to define laser-atom interactions. Time-independent Hamiltonians in the interaction picture are generated automatically from the specified atom, lasers and environment. Initial populations of atomic states, initial velocities and laser detunings can be passed as numpy arrays. The backend utilizes multi-threading and is written in C++ for the best performance and long-term support. Solvers for the rate equations, the Schrödinger equation and the master equation are available. Additionally, a Monte-Carlo master equation solver can be used to also simulate the recoil motion of the atom in the laser field. In `qspec.simulate`, an atom is defined as a list of states $|i\rangle := |\gamma, S, L, J, I, F, m_F\rangle$ with eigen energies $h\nu_i$ that are connected

through spontaneous decay rates Γ_{ij} . The eigen frequencies ν_i are either specified directly or calculated from the formulas for hyperfine-structure (hfs) and perturbative Zeeman shifts and

$$\nu_i = \nu_0 + \nu_{\text{hfs}} + \nu_{\text{Zeeman}} \quad (11)$$

$$\nu_{\text{hfs}} = A \frac{K}{2} + B \frac{\frac{3}{4}K(K+1) - I(I+1)J(J+1)}{2I(2I-1)J(2J-1)} + C \frac{\frac{5}{4}K^3 + 5K^2 + K(I(I+1) + J(J+1)) - 3I(I+1)J(J+1) + 3 - 5I(I+1)J(J+1)}{I(I-1)(2I-1)J(J-1)(2J-1)} \quad (12)$$

$$K := F(F+1) - I(I+1) - J(J+1) \quad (13)$$

$$\nu_{\text{Zeeman}} = -m_F g_F \frac{\mu_B}{h} \mathcal{B} \quad (14)$$

$$g_F = g_J \frac{F(F+1) + J(J+1) - I(I+1)}{2F(F+1)} + g_I \frac{\mu_N}{\mu_B} \frac{F(F+1) - J(J+1) + I(I+1)}{2F(F+1)} \quad (15)$$

$$g_J = -\frac{J(J+1) + L(L+1) - S(S+1)}{2J(J+1)} + g_s \frac{J(J+1) - L(L+1) + S(S+1)}{2J(J+1)}, \quad (16)$$

where A , B and C are the hyperfine-structure constants, \mathcal{B} is the external magnetic flux density, μ_B and μ_N are the Bohr and nuclear magneton, respectively, the Landé factor of the nucleus g_I has to be specified by the user and $g_s \approx -2.00232$. Lasers are approximated as classical monochromatic plane waves, for which the user specifies the frequency $\tilde{\nu}_k$, intensity I_k and complex polarization vector \vec{q}^k . The atom and the lasers are combined into an Interaction object which generates the differential equations to be solved. For a complete list of definitions for the mathematical objects used in `qspect.simulate`, see [Appendix B](#).

4.1. Hamiltonian

To simulate the coherent dynamics of the system, a Hamiltonian matrix is created in the basis of the atom, spanned by the user-specified states $|i\rangle$. The starting point is the time-dependent Hamiltonian

$$H = \sum_i \sigma_{ii} \hbar \omega_i + \sum_k \sum_{\substack{i,j \\ i \neq j}} \sigma_{ij} \hbar \Omega_{ij}^k \cos(\tilde{\omega}_k t), \quad (17)$$

where $\sigma_{ij} := |i\rangle\langle j|$, $\omega = 2\pi\nu$ are circular frequencies and Ω_{ij}^k are the Rabi frequencies. This Hamiltonian describes the interaction of an atom with multiple classical laser fields. In this form, every laser drives all atomic transitions σ_{ij} . The `qspect.simulate` module identifies the transitions that fulfill the electric-dipole-transition rules and calculates the Rabi frequencies from the parameters of the lasers and the properties of the involved atomic states. The full set of conditions for a

the center-of-gravity frequency ν_0 of the fine-structure states $|\gamma, S, L, J\rangle$ through [35]

transition σ_{ij} to be considered is given by

$$|J_j - J_i| \leq 1, \quad 0 \leftrightarrow 0 \quad (18)$$

$$|F_j - F_i| \leq 1, \quad 0 \leftrightarrow 0 \quad (19)$$

$$|m_j - m_i| \leq 1, \quad 0 \leftrightarrow 0 \quad \text{if } \Delta J, F = 0 \quad (20)$$

$$\Gamma_{ij} > 0 \quad (21)$$

$$I_k > 0 \quad (22)$$

$$(\vec{q}^k)_{m_j - m_i} \neq 0, \quad \nu_j > \nu_i \quad (23)$$

$$|\nu_j - \nu_i| - \tilde{\nu}_k \leq \Delta_{\text{max}}, \quad (24)$$

with the Einstein A_{ji} coefficient and a user-defined cutoff frequency Δ_{max} to ignore fast oscillations. Since the Hamiltonian still depends on the fast oscillating terms $\cos(\tilde{\omega}_k t)$, it is transformed into an interaction picture and the rotating-wave approximation is applied to frequencies of the order of $2\tilde{\omega}_k$. The transformation is defined to produce a time-independent Hamiltonian whenever possible to avoid complex exponentials for faster computation. This is possible if and only if two or more lasers do not form loops in the multigraph generated by connecting the atomic states with the lasers. Since the transformation depends on the particular graph, which is only determined at runtime, no closed expression for the transformed Hamiltonian can be specified. The graph search algorithm that is used for the transformation is described in Fig. 3 based on a laser-driven $^3S_1 \rightarrow ^3P_0$ transition in a system with nuclear spin $1/2$. The transformed time-independent Hamiltonian of this example is given by [36]

$$H' := U^\dagger H U + i\hbar \frac{dU^\dagger}{dt} U = \hbar(\omega_2 - \omega_0 - \tilde{\omega})(\hat{\sigma}_{22} + \hat{\sigma}_{33}) + \hbar \frac{\Omega}{2} (\hat{\sigma}_{02} + \hat{\sigma}_{13}) + \hbar \frac{\Omega^*}{2} (\hat{\sigma}_{20} + \hat{\sigma}_{31}), \quad (25)$$

where the indexes correspond to the states indicated in the simplified graph in Fig. 3, $\tilde{\omega}$ and Ω are the laser and Rabi frequencies, respectively, U is the unitary transformation defined in

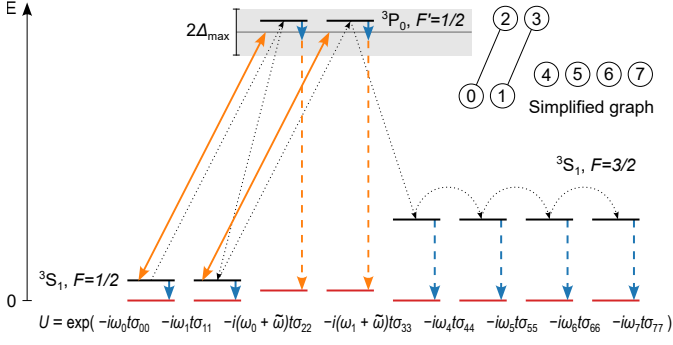


Figure 3: Sketch of the algorithm used to transform the Hamiltonian into the interaction picture for a laser-driven ${}^3S_1 \rightarrow {}^3P_0$ transition in a nuclear spin-1/2 system. The solid black and red lines depict the energies of the atomic states (diagonal elements of the Hamiltonian) before and after the transformation, respectively. The solid orange arrows depict the lasers, which are slightly detuned from resonance. The dashed arrows indicate the transformations applied to each state. The transformations applied to the ${}^3S_1 (F = 1/2)$ states (small dashed blue arrows) are carried over to the 3P_0 states due to the connection through the laser. Additionally, the 3P_0 states are shifted by the laser frequency $\tilde{\omega}$ (dashed orange arrow). The dotted black arrows show the path taken by the graph search algorithm. Note that this path changes, *e.g.*, if the maximum detuning Δ_{\max} is large enough to bring the laser in resonance with the $F = 3/2 \rightarrow F' = 1/2$ transition.

Fig. 3, and $\omega_0 = \omega_1$ as well as $\omega_2 = \omega_3$ due to the absence of an external magnetic field. When the time-dependence cannot be eliminated completely in the presence of multiple lasers, the off-diagonal elements of the Hamiltonian will contain time-dependent Rabi frequencies, which oscillate with the frequency differences between the lasers. This is automatically detected by the algorithm and the Hamiltonian is adjusted accordingly.

4.2. Lindblad Master equation

The complete coherent and dissipative population dynamics of the atomic states in the laser fields can be determined by solving the Lindblad master equation. It can be written as [36–38]

$$\frac{\partial \rho}{\partial t} = -\frac{i}{\hbar} [H, \rho] + \sum_{i,j} \Gamma_{ij} \mathcal{D}[\sigma_{ij}] \rho \quad (26)$$

$$\mathcal{D}[\sigma] \rho := \sigma \rho \sigma^\dagger - \frac{1}{2} (\sigma^\dagger \sigma \rho + \rho \sigma^\dagger \sigma), \quad (27)$$

where the coherent dynamics are described by the first term and the coupling to the vacuum by the second term. Note that $\Gamma_{ij} \neq 0 \Rightarrow \Gamma_{ji} = 0$ as spontaneous decay from $|i\rangle$ to $|j\rangle$ only occurs if $\omega_i > \omega_j$. In `qspect.simulate`, the differential Eq. (26) is solved numerically in matrix form using the C++ libraries `Boost.Numeric.Odeint` and `Eigen`. Large parameter spaces or numbers of samples can be explored by specifying frequency detunings, velocities (Doppler shifts) or initial density matrices (state populations) as `numpy` arrays, which are addressed in parallel by the C++ backend. Hence, a user is neither required to write any loops in Python nor to implement parallel computing. The performance of the master equation solvers in `qspect` and `qutip` for a single parameter sample are comparable and mainly depend on the chosen integration algorithm, integration steps and error tolerances.

A Monte-Carlo master equation solver is available, following the approach described in [39], which is also implemented in `qutip` [28]. The basic idea is to solve the Schrödinger equation with a modified non-hermitian Hamiltonian that leaks population into the environment according to the dissipation rates Γ_{ij} . Whenever the norm of a simulated state vector $|\psi_s\rangle$, where s numerates the samples, falls below a randomly generated fraction of unity, the state vector “collapses”, destroying all superpositions and resetting the system to the collapsed state. Averaging the resulting state vectors for $n \rightarrow \infty$ samples yields the density matrix described by the master equation

$$\rho_{ij} = \lim_{n \rightarrow \infty} \frac{1}{n} \sum_{s=1}^n \langle i | \psi_s \rangle \langle \psi_s | j \rangle. \quad (28)$$

The Monte-Carlo method is particularly useful for large atomic systems since its complexity only increases linearly with the number of atomic states as opposed to the quadratic growth of the master equation. In `qspect.simulate`, the Monte-Carlo master equation additionally can be used to simulate the motional degrees of freedom of the atom. Whenever the atom spontaneously decays, the photon momenta of the lasers leading from the initial to the excited state and the recoil from the spontaneous decay are added to the momentum of the atom. Note that with this method the momentum of the atom only changes upon spontaneous decays but not during any coherent interaction.

4.3. Rate equations

A simplification of the master equation are the rate equations which omit all coherent dynamics. In laser spectroscopy, the use of rate equations is often sufficient due to how precise the state populations need to be known or due to the width of the velocity distribution of the atomic ensemble, which can average out coherent effects. The rate equations implemented in `qspect.simulate` are given by

$$\frac{\partial \rho_{ii}}{\partial t} = \sum_j \left[\left(\sum_k R_{ij}^k \right) (\rho_{jj} - \rho_{ii}) + \Gamma_{ij} \rho_{jj} - \Gamma_{ji} \rho_{ii} \right], \quad (29)$$

where R_{ij}^k are the stimulated emission/absorption rates for laser k , which depend on the frequency, intensity and polarization of the laser, Γ_{ij} are the spontaneous decay rates from Eq. (26) and $\rho_{ij} = 0$ for $i \neq j$.

4.4. Differential scattering rate

From the density matrices determined through Eq. (26), (28) and (29), a differential scattering rate into the solid angle Ω can be calculated that, in case of the coherent approaches, also considers quantum interference effects. The differential scattering rate is given by [40]

$$\begin{aligned} \frac{d\Gamma}{d\Omega}(\vec{k}_{sc}) &:= \text{Tr}(\rho D(\vec{k}_{sc})) \\ &= \frac{1}{4\pi} \sum_{\vec{q} \in \mathcal{P}(\vec{k}_{sc})} \sum_{f \in \mathcal{F}} \sum_{i,j \in \mathcal{I}_f} \sqrt{\Gamma_{fi} \Gamma_{fj}} \frac{(\vec{q} \cdot \vec{d}_{fi})(\vec{d}_{fj}^* \cdot \vec{q}^*)}{\vec{d}_{fi} \cdot \vec{d}_{fj}^*} \rho_{ij}^*, \quad (30) \end{aligned}$$

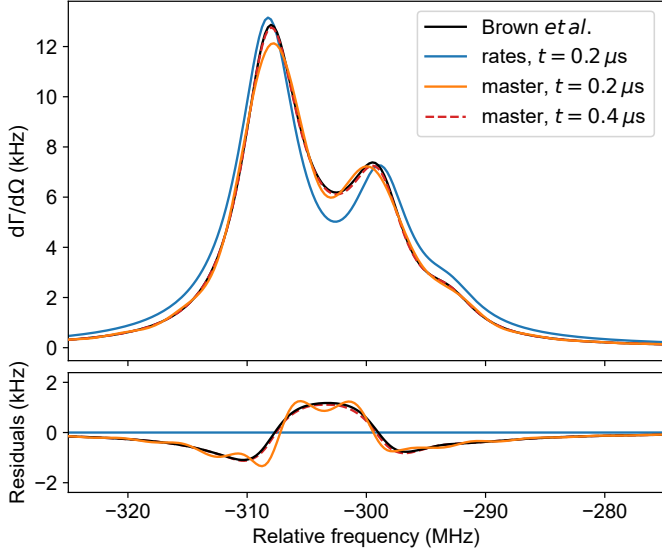


Figure 4: Simulated differential scattering rate of the $^2S_{1/2}(F=2) \rightarrow ^2P_{3/2}$ transitions in ^7Li in the direction of the linear polarization vector of a spectroscopy laser with an intensity of $1 \mu\text{W}/\text{mm}^2$. The perturbative scattering rate, which includes quantum interference (QI) effects derived by Brown *et al.* [26] (black) is compared to the solutions of the rate (blue) and master (orange) equations after an integration time of $0.2 \mu\text{s}$. While the rate equations yield a sum of Lorentzians with averaged out coherent and QI effects, the master equation approach shows the intensity modulations of the coherent Rabi oscillations and converges to the perturbative QI approach for later times (red dashed). A small difference comes from optical population transfer into the $F=1$ ground state. This plot reproduces Fig. 2 of [26]. The shown data was generated using Code Listing 1.

where $D(\vec{k}_{\text{sc}})$ is a detection operator, $\mathcal{P}(\vec{k}_{\text{sc}})$ is a basis set of normalized polarization vectors for scattered photons with direction \vec{k}_{sc} , $(I_f)_{f \in \mathcal{F}}$ and \mathcal{F} are sets of excited and final states between which spontaneous decay can occur and \vec{d} are the dipole transition strengths, see Eq. (B.4). Limiting the three sums to detectable spontaneous decay and integrating over the solid angle of detection yields a photon detection rate.

Equation (30) reproduces the perturbative differential scattering rate derived by Brown *et al.* [26] that considers quantum interference effects in closed electronic transitions in the case of small laser intensities, where $\Omega_{ij} \ll \Gamma_{ij}$, linear polarization and equilibrium ground-state population. These conditions are rarely met exactly in the experiment as in most real atomic systems, especially if they have a hyperfine structure, optical pumping and population transfer will occur already within short interaction times and laser powers on the $\mu\text{W}/\text{mm}^2$ level. A comparison of differential scattering rates of the $^2S_{1/2} \rightarrow ^2P_{3/2}$ transition in ^7Li is shown in Fig. 4. The scattering rates were determined with Eq. (30) using the master and the rate equation approaches as well as with the perturbative scattering rate from [26] for detection at 0° angle relative to the polarization vector of absorbed photons. A code example that produces the data shown in Fig. 4 is given in Code Listing 1. The shown plot reproduces Fig. 2 from [26] and additionally shows the solution of the master equation approach after an integration time of $0.2 \mu\text{s}$, demonstrating the need of the non-perturbative approach if the system equilibrium is not reached yet.

5. Summary and outlook

The Python package `qspect` provides a variety of classes and functions to facilitate the analysis and simulation workflow in laser spectroscopy experiments. In this article, a multidimensional linear regression algorithm, modular fit models and light-matter simulations are introduced. The maximum-likelihood fit of a straight line in multiple dimensions constitutes a generalization of the linear regression algorithm introduced by York *et al.* [22]. The system of modular fit models provides a basis for combining and linking different fit models, parameters and data sets and can be easily expanded with new models. The simulation module for coherent light-matter interactions offers an intuitive and user-friendly interface without the need to specify a Hamiltonian or other complicated mathematical objects.

The `qspect` package is built to be as general as possible within the given set of physical conditions. An expansion of `qspect` with new features and further generalization for a larger scope of applications is planned. For example, the simulation module can be used to define a new lineshape model for fitting, which can account for the population dynamics of an atom in a laser field. The simulation module itself can be expanded, *e.g.*, by accounting for finite laser linewidths, adding molecular systems or allowing higher-order multipole transition or time-dependent velocities and laser parameters.

Acknowledgements

We thank K. König, B. Maaß, E. Matthews, K. Mohr, L. Renth and J. Spahn for testing the `qspect` package and their valuable feedback. We acknowledge support by the Deutsche Forschungsgemeinschaft (DFG, German Research Foundation) under - Projektnummer 279384907 - SFB 1245, and the BMBF under Contract No. 05P19RDFN1. P. M. acknowledges support from HGS-HIRE.

Code Listing 1: Example code to produce the data shown in Fig. 4. Lists of the magnetic substates of the ground (s) and the excited state (p) are created (line 11-14), connected in a DecayMap (line 16) and used to define a ^7Li atom (line 17). A laser is defined with an intensity of $1 \mu/\text{mm}^2$ and π -polarized light (line 19-21). An Interaction object combines the atom and a list of lasers (line 23). The rate (line 30) and master (line 33) equation solvers are called directly from the Interaction object for an array of frequency detunings delta. The scattering rate for the different detunings defined in Eq. (30) is calculated directly from the array of density matrices rho or state populations n. An extended version of the perturbative scattering rate derived by Brown *et al.* [26] is calculated using a ScatteringRate object (line 36). Transition frequencies and hyperfine structure constants are taken or calculated from the data in [26]. The Einstein coefficient is taken from [41].

```

1 import numpy as np
2 import qspec as qs
3 import qspec.simulate as sim
4
5 f_sp = 446810183.163 # Transition frequency (MHz)
6 a_sp = 36.891 # Einstein coefficient (rad MHz)
7
8 s_hyper = [401.75825] # HFS constants (MHz)
9 p_hyper = [-3.055038, -0.29670]
10
11 s = sim.construct_electronic_state(
12     0., s=0.5, l=0, j=0.5, i=1.5, hyper_const=s_hyper, label='s')
13 p = sim.construct_electronic_state(
14     f_sp, s=0.5, l=1, j=1.5, i=1.5, hyper_const=p_hyper, label='p')
15
16 decay = sim.DecayMap(labels=[('s', 'p')], a=[a_sp])
17 li7 = sim.Atom(s + p, decay)
18
19 intensity = 1. # uW /mm**2
20 polarization = sim.Polarization([0, 1, 0]) # Linear polarization
21 laser = sim.Laser(f_sp, intensity, polarization)
22
23 inter = sim.Interaction(li7, [laser])
24 inter.controlled = True # Error controlled integrator
25
26 t = 0.2 # Integration time (us)
27 delta = np.linspace(-325, -275, 201) # Frequency detunings (MHz)
28 theta, phi = 0., 0. # Angles from z-axis in x- and y-direction (rad)
29
30 n = inter.rates(t, delta) # Rate equations
31 y_rates = li7.scattering_rate(n, theta, phi, as_density_matrix=False)
32
33 rho = inter.master(t, delta) # Master equation
34 y_master = li7.scattering_rate(rho, theta, phi)
35
36 sr = sim.ScatteringRate(li7, laser=laser)
37 y_brown = sr.generate_y(delta, theta, phi)[: , 0, 0] # Brown et al.

```

Appendix A. Gradient and Hessian of the negated log-likelihood function

For the minimization of the negative log-likelihood function given by Eq. (7), its gradient vector and Hessian are calculated analytically. Both are used in the Newton conjugate gradient (Newton-CG) method [16, 31] and the Hessian is also used to estimate the covariance matrix of the resulting parameters. We define

$$\tilde{a}_{ij} := (\Sigma_i^{-1} \vec{a}_i)_j, \quad \tilde{b}_{ij} := (\Sigma_i^{-1} \vec{b}_i)_j. \quad (\text{A.1})$$

Then the components of the gradient vector of Eq. (7) are given by

$$\frac{\partial}{\partial a_j} \mathcal{L} = \sum_{i \in \mathcal{I}} \left[\tilde{a}_{ij} - \frac{t_i}{\sigma_i^2} \tilde{b}_{ij} \right] \quad (\text{A.2})$$

$$\frac{\partial}{\partial b_j} \mathcal{L} = \sum_{i \in \mathcal{I}} \left[\frac{t_i}{\sigma_i^2} \tilde{a}_{ij} - \frac{t_i^2}{\sigma_i^4} \tilde{b}_{ij} \right], \quad (\text{A.3})$$

and the components of the Hessian are given by

$$\frac{\partial^2}{\partial a_j \partial a_l} \mathcal{L} = \sum_{i \in \mathcal{I}} \left[(\Sigma_i^{-1})_{jl} - \frac{\tilde{b}_{ij} \tilde{b}_{il}}{\sigma_i^2} \right] \quad (\text{A.4})$$

$$\begin{aligned} \frac{\partial^2}{\partial b_j \partial b_l} \mathcal{L} = \sum_{i \in \mathcal{I}} \left[\frac{t_i^2}{\sigma_i^4} (\Sigma_i^{-1})_{jl} - \frac{1}{\sigma_i^2} \tilde{a}_{ij} \tilde{a}_{il} - 4 \frac{t_i^2}{\sigma_i^6} \tilde{b}_{ij} \tilde{b}_{il} \right. \\ \left. + 2 \frac{t_i}{\sigma_i^4} (\tilde{a}_{ij} \tilde{b}_{il} + \tilde{b}_{ij} \tilde{a}_{il}) \right] \end{aligned} \quad (\text{A.5})$$

$$\frac{\partial^2}{\partial a_j \partial b_l} \mathcal{L} = \sum_{i \in \mathcal{I}} \left[-\frac{t_i^2}{\sigma_i^2} (\Sigma_i^{-1})_{jl} + 2 \frac{t_i}{\sigma_i^4} \tilde{b}_{ij} \tilde{b}_{il} - \frac{1}{\sigma_i^2} \tilde{a}_{ij} \tilde{b}_{il} \right]. \quad (\text{A.6})$$

Appendix B. Definitions for `qspec.simulate`

The following definitions are used to calculate light-matter interactions in `qspec.simulate` [26, 42]

$$\begin{aligned} a_{ij} = (-1)^{I+J_j+F_i+1} \sqrt{2F_i+1} \sqrt{2J_j+1} \\ \times \langle F_i m_i; 1 m_j - m_i | F_j m_j \rangle \begin{Bmatrix} J_j & J_i & 1 \\ F_i & F_j & I \end{Bmatrix} \end{aligned} \quad (\text{B.1})$$

$$\tilde{\Gamma}_{ij} = \begin{cases} A_{ji} & \omega_i < \omega_j \\ A_{ij} & \text{else} \end{cases} \quad (\text{B.2})$$

$$\Gamma_{ij} = a_{ij}^2 A_{ji} \quad (\text{B.3})$$

$$d_{ij} = \sqrt{\frac{3\pi\epsilon_0 c^3 \hbar \tilde{\Gamma}_{ij}}{\omega_{ij}^3}} a_{ij} \quad (\text{B.4})$$

$$M_{ij}^k = \begin{cases} 1 & \text{Eq. (18) - (24) fulfilled} \\ 0 & \text{else} \end{cases} \quad (\text{B.5})$$

$$\Omega_{ij}^k = \sqrt{\frac{2I_k}{\epsilon_0 c}} \frac{d_{ij} (\vec{q}^k)_{m_j - m_i}}{\hbar} M_{ij}^k \quad (\text{B.6})$$

$$R_{ij}^k = \frac{|\Omega_{ij}^k|^2 \tilde{\Gamma}_{ji}}{(\tilde{\omega}_k - |\omega_j - \omega_i|)^2 + \frac{1}{4} \tilde{\Gamma}_{ji}^2}, \quad (\text{B.7})$$

where $\langle \dots | \dots \rangle$ are the Clebsch-Gordan coefficients, $\{:::\}$ are the Wigner-6j symbols, \vec{q}^k is a normalized complex laser polarization vector of laser k , A_{ji} are Einstein coefficients, I_k are the laser intensities, ϵ_0 is the vacuum permittivity and c is the velocity of light.

References

- [1] R. Neugart, Laser spectroscopy on mass-separated radioactive beams, Nuclear Instruments and Methods in Physics Research 186 (1981) 165–175. doi:10.1016/0029-554X(81)90902-2.
- [2] E. W. Otten, Nuclear Radii and Moments of Unstable Isotopes, in: D. A. Bromley (Ed.), Treatise on Heavy Ion Science, Springer Boston, 1989, pp. 517–638. doi:10.1007/978-1-4613-0713-6_7.
- [3] K. Blaum, J. Dilling, W. Nörtershäuser, Precision atomic physics techniques for nuclear physics with radioactive beams, Physica Scripta T152 (2013) 014017. doi:10.1088/0031-8949/2013/T152/014017.
- [4] P. Campbell, I. D. Moore, M. R. Pearson, Laser spectroscopy for nuclear structure physics, Progress in Particle and Nuclear Physics 86 (2016) 127–180. doi:10.1016/j.pnpnp.2015.09.003.
- [5] J. Ullmann, Z. Andelkovic, C. Brandau, A. Dax, W. Geithner, C. Geppert, C. Gorges, M. Hammen, V. Hannen, S. Kaufmann, K. König, Y. A. Litvinov, M. Lochmann, B. Maaß, J. Meisner, T. Murböck, R. Sánchez, M. Schmidt, S. Schmidt, M. Steck, T. Stöhlker, R. C. Thompson, C. Trageser, J. Vollbrecht, C. Weinheimer, W. Nörtershäuser, High precision hyperfine measurements in Bismuth challenge bound-state strong-field QED, Nature Communications 8 (2017) 15484. doi:10.1038/ncomms15484.
- [6] P. Müller, K. König, P. Imgram, J. Krämer, W. Nörtershäuser, Collinear laser spectroscopy of Ca^+ : Solving the field-shift puzzle of the $4s^2S_{1/2} \rightarrow 4p^2P_{1/2,3/2}$ transitions, Physical Review Research 2 (2020) 043351. doi:10.1103/PhysRevResearch.2.043351.
- [7] J. J. Hudson, D. M. Kara, I. J. Smallman, B. E. Sauer, M. R. Tarbutt, E. A. Hinds, Improved measurement of the shape of the electron, Nature 473 (2011) 493–496. doi:10.1038/nature10104.
- [8] M. S. Safronova, D. Budker, D. DeMille, D. F. J. Kimball, A. Derevianko, C. W. Clark, Search for new physics with atoms and molecules, Reviews of Modern Physics 90 (2018) 025008. doi:10.1103/RevModPhys.90.025008.
- [9] B. J. Bloom, T. L. Nicholson, J. R. Williams, S. L. Campbell, M. Bishof, X. Zhang, W. Zhang, S. L. Bromley, J. Ye, An optical lattice clock with accuracy and stability at the 10^{-18} level, Nature 506 (2014) 71–75. doi:10.1038/nature12941.
- [10] A. D. Ludlow, M. M. Boyd, J. Ye, E. Peik, P. O. Schmidt, Optical atomic clocks, Reviews of Modern Physics 87 (2015) 637–701. doi:10.1103/RevModPhys.87.637.
- [11] S. L. Campbell, R. B. Hutson, G. E. Marti, A. Goban, N. Darkwah Opong, R. L. McNally, L. Sonderhouse, J. M. Robinson, W. Zhang, B. J. Bloom, J. Ye, A Fermi-degenerate three-dimensional optical lattice clock, Science 358 (2017) 90–94. doi:10.1126/science.aam5538.
- [12] J. I. Cirac, P. Zoller, Quantum Computations with Cold Trapped Ions, Physical Review Letters 74 (1995) 4091–4094. doi:10.1103/PhysRevLett.74.4091.
- [13] H. Häffner, C. Roos, R. Blatt, Quantum computing with trapped ions, Physics Reports 469 (2008) 155–203. doi:10.1016/j.physrep.2008.09.003.
- [14] N. Friis, O. Marty, C. Maier, C. Hempel, M. Holzäpfel, P. Jurcevic, M. B. Plenio, M. Huber, C. Roos, R. Blatt, B. Lanyon, Observation of Entangled States of a Fully Controlled 20-Qubit System, Physical Review X 8 (2018) 021012. doi:10.1103/PhysRevX.8.021012.
- [15] C. R. Harris, K. J. Millman, S. J. van der Walt, R. Gommers, P. Virtanen, D. Cournapeau, E. Wieser, J. Taylor, S. Berg, N. J. Smith, R. Kern, M. Picus, S. Hoyer, M. H. van Kerkwijk, M. Brett, A. Haldane, J. F. Del Río, M. Wiebe, P. Peterson, P. Gérard-Marchant, K. Sheppard, T. Reddy, W. Weckesser, H. Abbasi, C. Gohlke, T. E. Oliphant, Array programming with NumPy, Nature 585 (2020) 357–362. doi:10.1038/s41586-020-2649-2.
- [16] P. Virtanen, R. Gommers, T. E. Oliphant, M. Haberland, T. Reddy, D. Cournapeau, E. Burovski, P. Peterson, W. Weckesser, J. Bright, S. J.

- van der Walt, M. Brett, J. Wilson, K. J. Millman, N. Mayorov, A. R. J. Nelson, E. Jones, R. Kern, E. Larson, C. J. Carey, Í. Polat, Y. Feng, E. W. Moore, J. VanderPlas, D. Laxalde, J. Perktold, R. Cimrman, I. Henriksen, E. A. Quintero, C. R. Harris, A. M. Archibald, A. H. Ribeiro, F. Pedregosa, P. van Mulbregt, SciPy 1.0: fundamental algorithms for scientific computing in Python, *Nature Methods* 17 (2020) 261–272. doi:10.1038/s41592-019-0686-2.
- [17] A. Meurer, C. P. Smith, M. Paprocki, O. Čertík, S. B. Kirpichev, M. Rocklin, A. Kumar, S. Ivanov, J. K. Moore, S. Singh, T. Rathnayake, S. Vig, B. E. Granger, R. P. Muller, F. Bonazzi, H. Gupta, S. Vats, F. Johansson, F. Pedregosa, M. J. Curry, A. R. Terrel, Š. Roučka, A. Saboo, I. Fernando, S. Kulal, R. Cimrman, A. Scopatz, SymPy: symbolic computing in Python, *PeerJ Computer Science* 3 (2017) e103. doi:10.7717/peerj-cs.103.
- [18] J. D. Hunter, Matplotlib: A 2D Graphics Environment, *Computing in Science & Engineering* 9 (2007) 90–95. doi:10.1109/MCSE.2007.55.
- [19] P. Müller, *qspect*. URL <https://pypi.org/project/qspect/>
- [20] P. Müller, Laserspectroscopic determination of the nuclear charge radius of ^{13}C , Doctoral thesis (PhD thesis), Technische Universität Darmstadt (2024). doi:10.26083/tuprints-00026746.
- [21] W. H. King, *Isotope Shifts in Atomic Spectra*, Springer New York, 1984. doi:10.1007/978-1-4899-1786-7.
- [22] D. York, N. M. Evensen, M. L. MartíÁñez, J. de Basabe Delgado, Unified equations for the slope, intercept, and standard errors of the best straight line, *American Journal of Physics* 72 (2004) 367–375. doi:10.1119/1.1632486.
- [23] F. Gebert, Y. Wan, F. Wolf, C. N. Angstromann, J. C. Berengut, P. O. Schmidt, Precision Isotope Shift Measurements in Calcium Ions Using Quantum Logic Detection Schemes, *Physical Review Letters* 115 (2015) 053003. doi:10.1103/PhysRevLett.115.053003.
- [24] W. Gins, R. P. de Groote, M. L. Bissell, C. Granados Buitrago, R. Ferrer, K. M. Lynch, G. Neyens, S. Sels, Analysis of counting data: Development of the SATLAS Python package, *Computer Physics Communications* 222 (2018) 286–294. doi:10.1016/j.cpc.2017.09.012.
- [25] W. Gins, B. van den Borne, R. P. de Groote, G. Neyens, SATLAS2: An update to the package for analysis of counting data, *Computer Physics Communications* 297 (2024) 109053. doi:10.1016/j.cpc.2023.109053.
- [26] R. C. Brown, S. Wu, J. V. Porto, C. J. Sansonetti, C. E. Simien, S. M. Brewer, J. N. Tan, J. D. Gillaspay, Quantum interference and light polarization effects in unresolvable atomic lines: Application to a precise measurement of the $^{6,7}\text{Li } D_2$ lines, *Physical Review A* 87 (2013) 032504. doi:10.1103/PhysRevA.87.032504.
- [27] W. R. Johnson, K. T. Cheng, D. R. Plante, Hyperfine structure of 2^3P levels of heliumlike ions, *Physical Review A* 55 (1997) 2728–2742. doi:10.1103/PhysRevA.55.2728.
- [28] J. R. Johansson, P. D. Nation, F. Nori, QuTiP: An open-source Python framework for the dynamics of open quantum systems, *Computer Physics Communications* 183 (2012) 1760–1772. doi:10.1016/j.cpc.2012.02.021.
- [29] J. R. Johansson, P. D. Nation, F. Nori, QuTiP 2: A Python framework for the dynamics of open quantum systems, *Computer Physics Communications* 184 (2013) 1234–1240. doi:10.1016/j.cpc.2012.11.019.
- [30] S. Eckel, D. S. Barker, E. B. Norrgard, J. Scherschligt, PyLCP: A Python package for computing laser cooling physics, *Computer Physics Communications* 270 (2020) 108166. doi:10.1016/j.cpc.2021.108166.
- [31] J. Nocedal, S. J. Wright, *Numerical Optimization*, Springer New York, 2006. doi:10.1007/978-0-387-40065-5.
- [32] S. Kaufmann, *Laser spectroscopy of nickel isotopes with a new data acquisition system at ISOLDE*, Doctoral thesis (PhD thesis), Technische Universität Darmstadt (2019). URL <https://tuprints.ulb.tu-darmstadt.de/id/eprint/9286>
- [33] S. Malbrunot-Ettenauer, S. Kaufmann, S. Bacca, C. Barbieri, J. Billowes, M. L. Bissell, K. Blaum, B. Cheal, T. Duguet, R. F. G. Ruiz, W. Gins, C. Gorges, G. Hagen, H. Heylen, J. D. Holt, G. R. Jansen, A. Kanelakopoulos, M. Kortelainen, T. Miyagi, P. Navrátil, W. Nazarewicz, R. Neugart, G. Neyens, W. Nörtershäuser, S. J. Novario, T. Papenbrock, T. Ratajczyk, P.-G. Reinhard, L. V. Rodríguez, R. Sánchez, S. Sailer, A. Schwenk, J. Simonis, V. Somà, S. R. Stroberg, L. Wehner, C. Wraith, L. Xie, Z. Y. Xu, X. F. Yang, D. T. Yordanov, Nuclear Charge Radii of the Nickel Isotopes $^{58-68,70}\text{Ni}$, *Physical Review Letters* 128 (2022) 022502. doi:10.1103/PhysRevLett.128.022502.
- [34] P. Müller, S. Kaufmann, T. Miyagi, J. Billowes, M. L. Bissell, K. Blaum, B. Cheal, R. F. Garcia Ruiz, W. Gins, C. Gorges, H. Heylen, A. Kanelakopoulos, S. Malbrunot-Ettenauer, R. Neugart, G. Neyens, W. Nörtershäuser, T. Ratajczyk, L. V. Rodríguez, R. Sánchez, S. Sailer, A. Schwenk, L. Wehner, C. Wraith, L. Xie, Z. Y. Xu, X. F. Yang, D. T. Yordanov, Electromagnetic moments of the odd-mass nickel isotopes $^{59-67}\text{Ni}$, *Physics Letters B* 854 (2024) 138737. doi:10.1016/j.physletb.2024.138737.
- [35] R. P. de Groote, S. Kujanpää, Á. Koszorús, J. G. Li, I. D. Moore, Magnetic octupole moment of ^{173}Yb using collinear laser spectroscopy, *Physical Review A* 103 (2021) 032826. doi:10.1103/PhysRevA.103.032826.
- [36] D. Manzano, A short introduction to the Lindblad master equation, *AIP Advances* 10 (2020) 025106. doi:10.1063/1.5115323.
- [37] G. Lindblad, On the generators of quantum dynamical semigroups, *Communications in Mathematical Physics* 48 (1976) 119–130. doi:10.1007/BF01608499.
- [38] H. J. Carmichael, *Statistical Methods in Quantum Optics 1*, Springer Berlin Heidelberg, 1999. doi:10.1007/978-3-662-03875-8.
- [39] R. Dum, P. Zoller, H. Ritsch, Monte Carlo simulation of the atomic master equation for spontaneous emission, *Physical Review A* 45 (1992) 4879–4887. doi:10.1103/PhysRevA.45.4879.
- [40] G. Drake, *Springer Handbook of Atomic, Molecular, and Optical Physics*, Springer New York, 2006. doi:10.1007/978-0-387-26308-3.
- [41] A. Kramida, Y. Ralchenko, J. Reader, NIST ASD Team, NIST Atomic Spectra Database (ver. 5.10). doi:10.18434/T4W30F.
- [42] R. C. Hilborn, Einstein coefficients, cross sections, f values, dipole moments, and all that, *American Journal of Physics* 50 (1982) 982–986. doi:10.1119/1.12937.